The multivariate analysis revealed that WBRT + SRS was associated with a reduced risk of recurrence (hazard ratio, 0.32; 95% CI, 0.18-0.58; $P<.001$) (TABLE 5 and TABLE 6).

During the follow-up period, 122 patients (92% of the total patients enrolled) had at least 1 follow-up MRI scan performed. In total, 581 follow-up MRI scans were performed; of these, 87 scans (15%) demonstrated new brain metastases; these 87 "event scans" were obtained in 55 patients. Sixteen percent of these "event scans" (14/87) were associated with neurologic symptoms at the time of the MRI examination.

A total of 247 metastases received initial treatment with SRS (117 in the WBRT + SRS group and 130 in the SRS-alone group). Follow-up MRI was available for 210 metastases (85%). The actuarial local tumor control rate at 12 months was 88.7% (95% CI, 80.1%-97.3%) in the WBRT + SRS group and 72.5% (95% CI, 60.3%-84.7%) in the SRS-alone group ($P=.002$) (FIGURE 3). The histopathological type (adenocarcinoma vs others) was not shown to be a significant factor ($P=.90$). The multivariate analysis also showed significantly better tumor control by WBRT + SRS treatment (hazard ratio, 4.83; 95% CI, 2.00-11.65; $P<.001$).

Salvage treatment for progression of brain tumor was required significantly more frequently in patients receiving SRS alone (29 patients) than in the WBRT + SRS group (10 patients) ($\chi^2=12.33$; $P<.001$). Salvage WBRT was applied in 11 patients in the SRS-alone group but was not used in any patients in the WBRT + SRS group. Salvage SRS was used in 19 patients in the SRS-alone group and in 9 patients in the WBRT + SRS group.

## Systemic and Neurologic Functional Preservation

Systemic functional preservation rates (KPS score $\geq70$) at 12 months were 33.9% (95% CI, 22.2%-45.4%) in the WBRT + SRS group and 26.9% (95% CI, 16.3%-37.5%) in the SRS-alone group ($P=.53$). The decrease in the KPS score to below 70 was attributed to neurologic causes in 17 patients (29%) in the WBRT + SRS group and 14 (22%) in the SRS-alone group.

The actuarial rates of neurologic preservation at 12 months were 72.1% (95% CI, 58.8%-85.4%) with WBRT + SRS and 70.3% (95% CI, 55.6%-85.0%) with SRS alone ($P=.99$) when neurologic preservation was defined as a lack of any worsening of the neurologic grade on follow-up examination, compared with the pretreatment grade. In total, 85 patients (38 in the WBRT + SRS group and 47 in the SRS-alone group) did not have neurologic symptoms when brain metastases were diagnosed (grade 0). Among the 47 patients who had a pretreatment grade of 1 to 3, an improvement in neurologic status was observed at least once in 9 patients and 10 patients in the respective groups ($\chi^2=1.32$; $P=.24$). Deterioration of neurologic function was observed in 43 patients, including 7 who initially experienced improvement after treatment (22 in the WBRT + SRS group and 21 in the SRS-alone group; $\chi^2=0.09$; $P=.75$). This deterioration was attributed to either original or distant brain metastases in 13 patients (59%) in the WBRT + SRS group and 18 patients (86%) in the SRS-alone group ($\chi^2=3.78$; $P=.05$).

Late neurologic radiation toxic effects were the cause of deterioration in 4 and 2 patients in each group, respectively. Either meningeal dissemination or spinal cord metastases induced neurologic deterioration in 5 and 1 patient in each group, respectively.
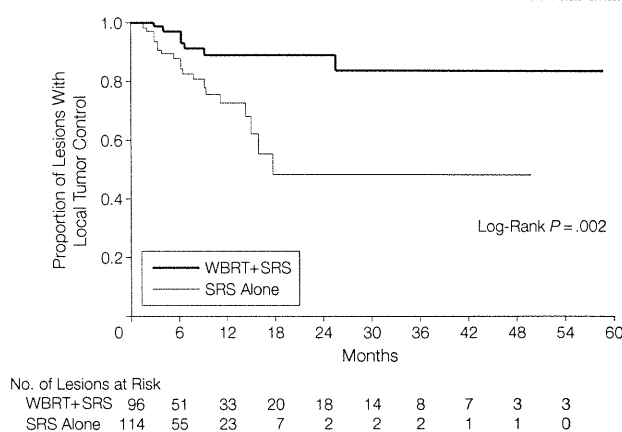
Neurocognitive function was optionally assessed using the Mini-Mental State Examination (MMSE). Among the 44 patients (25 in the WBRT + SRS group and 19 in the SRS-alone group) who lived 12 months or longer, MMSE data were available in 28 patients at least once (16 in the WBRT + SRS group and 12 in the SRS-alone group) at the median follow-up times of 30.5 months (range, 13.7-58.7 months) with WBRT + SRS and 20.7 months (range, 13.3-53.8 months) with SRS alone. The median MMSE pretreatment score was 28.0 (range, 23-30) in the WBRT + SRS

**Table 6.** Multivariate Analysis of Development of New Metastases at Distant Brain Sites

| | Hazard Ratio (95% CI) | P Value |
|---|---|---|
| Treatment group (WBRT + SRS) | 0.32 (0.18-0.58) | <.001 |
| No. of brain metastases (2-4) | 1.69 (0.97-2.93) | .06 |
| Extracranial metastases (active) | 2.06 (1.17-3.64) | .01 |
| KPS score (70-80) | 2.14 (1.17-3.93) | .01 |

Abbreviations: CI, confidence interval; KPS, Karnofsky Performance Status; SRS, stereotactic radiosurgery; WBRT, whole-brain radiation therapy.

**Figure 3.** Local Tumor Control



No. of Lesions at Risk

| | 0 | 6 | 12 | 18 | 24 | 30 | 36 | 42 | 48 | 54 | 60 |
|---|---|---|---|---|---|---|---|---|---|---|---|
| WBRT+SRS | 96 | 51 | 33 | 20 | 18 | 14 | 8 | 7 | 3 | 3 | |
| SRS Alone | 114 | 55 | 23 | 7 | 2 | 2 | 2 | 1 | 1 | 0 | |

There was a statistically significant increase in local tumor control in patients receiving whole-brain radiation therapy (WBRT) plus stereotactic radiosurgery (SRS) ($P=.002$).

— 82 —

group and 27.0 (range, 23-30) in the SRS-alone group. The median score at the final follow-up was 27.0 (range, 21-30) in the WBRT + SRS group and 28.0 (range, 18-30) in the SRS-alone group.

## COMMENT

Stereotactic radiosurgery is a method of delivering high doses of focal radiation to a tumor while minimizing irradiation of the adjacent normal tissue. This approach was originally developed by the Swedish neurosurgeon Lars Leksell as a substitute for direct surgical intervention.[21] Stereotactic radiosurgery is now available worldwide, and it is increasingly used to treat brain metastases because it is less invasive compared with direct surgical intervention, although a direct randomized comparison of the 2 modes has not been performed to date.

Whole-brain radiation therapy has been a standard treatment for brain metastases for several decades.[1-4,6,7,17] In more recent years, the importance of focal aggressive therapy combined with WBRT has been increasingly recognized.[3,4,22-24] Andrews et al[4] recently reported the results from RTOG 9508, a multi-institutional phase 3 trial of 333 patients with 1 to 3 brain metastases who received WBRT with or without SRS boost. A statistically significant improvement in median survival with the addition of SRS was seen in patients with a single brain metastasis.

To reduce the risk of late radiation effects,[1,2,5] WBRT is increasingly being omitted from the initial management strategy.[6-13] There is not yet a general consensus regarding the risks and benefits of omitting up-front WBRT. One study showed a trend toward improved survival among patients who received SRS alone,[12] whereas another study showed a trend toward worse survival among patients who received SRS alone.[10] A retrospective multi-institutional review of SRS alone vs SRS with WBRT in 569 patients failed to show any difference in survival between the 2 groups.[7] In a single-institution prospective randomized trial comparing WBRT with observation in

patients who underwent conventional surgery,[6] a large increase in intracranial relapse and a concomitant increase in death due to neurologic causes were identified in the non-WBRT group; however, no survival difference was identified in that study. In the present study, no significant survival difference was observed between the groups receiving WBRT + SRS and SRS alone, although the number of patients was not large enough to allow detection of any differences that were smaller than we had assumed. In addition, no significant difference in the frequency of death due to neurologic causes was observed. Moreover, these results were obtained in spite of the rather large increase in intracranial failure when WBRT was omitted. A further observation of note from the present trial was the significant increase in local failure with SRS alone, even though the radiation dose in these patients was considerably higher than that administered to patients receiving WBRT + SRS. We have adapted the 30% reduced dose of SRS in the WBRT + SRS group, which could have lowered local control of the brain metastasis in the WBRT + SRS group. However, we have observed opposite results in this study; the local control rate was significantly higher in the WBRT + SRS group than in the SRS-alone group. This observation lends merit to the value of fractionation, which might help overcome some radiation resistance mechanisms, such as hypoxia.

Also of concern in this context is that higher brain recurrence rates are associated with neurologic deterioration.[9] In a previous randomized study of surgery with or without WBRT,[6] the time to neurologic deterioration was dramatically longer in the WBRT group, although no difference in functional independence was observed. In the current study, no significant difference in the preservation of neurologic function was observed. However, the present study might have less ability to detect small differences, and the present assessment of neurologic function was not

conducted with sophisticated measures that might have detected differences between patient groups.

Although surgery and SRS are both focal treatments, SRS is less invasive and may be repeated more often than surgical intervention.[11] The optimal timing of these interventions is an issue that remains open for debate. Our results suggest that the early detection of a brain recurrence and early salvage brain treatment may prevent neurologic deterioration and neurologic death, even when WBRT is not included in the initial treatment. However, study participants more frequently undergo physical and radiological examinations than do patients in the community. Given that the majority of new brain metastases were initially detected in asymptomatic patients, studies assessing the benefits of scheduled imaging should be conducted in the future.

In conclusion, our findings demonstrated that SRS alone without up-front WBRT was associated with increased brain tumor recurrence; however, it did not result in either worsened neurologic function or increased risk of neurologic death. With respect to patient survival, the control of systemic cancer might outweigh the frequent recurrence of brain tumors. Therefore, SRS alone could be a treatment option, provided that frequent monitoring of brain tumor status is conducted.

— 83 —

## REFERENCES

1. Patchell RA. The management of brain metastases. *Cancer Treat Rev*. 2003;29:533-540.
2. Bradley KA, Mehta MP. Management of brain metastases. *Semin Oncol*. 2004;31:693-701.
3. Kondziolka D, Patel A, Lunsford LD, Kassam A, Flickinger JC. Stereotactic radiosurgery plus whole brain radiotherapy versus radiotherapy alone for patients with multiple brain metastases. *Int J Radiat Oncol Biol Phys*. 1999;45:427-434.
4. Andrews DW, Scott CB, Sperduto PW, et al. Whole brain radiation therapy with or without stereotactic radiosurgery boost for patients with one to three brain metastases: phase III results of the RTOG 9508 randomised trial. *Lancet*. 2004;363:1665-1672.
5. DeAngelis LM, Delattre JY, Posner JB. Radiation-induced dementia in patients cured of brain metastases. *Neurology*. 1989;39:789-796.
6. Patchell RA, Tibbs PA, Regine WF, et al. Postoperative radiotherapy in the treatment of single metastases to the brain. *JAMA*. 1998;280:1485-1489.
7. Sneed PK, Suh JH, Goetsch SJ, et al. A multi-institutional review of radiosurgery alone vs radiosurgery with whole brain radiotherapy as the initial management of brain metastases. *Int J Radiat Oncol Biol Phys*. 2002;53:519-526.
8. Flickinger JC, Kondziolka D, Lunsford LD, et al. A multi-institutional experience with stereotactic radiosurgery for solitary brain metastasis. *Int J Radiat Oncol Biol Phys*. 1994;28:797-802.
9. Regine WF, Huhn JL, Patchell RA, et al. Risk of symptomatic brain tumor recurrence and neurologic deficit after radiosurgery alone in patients with newly diagnosed brain metastases: results and implications. *Int J Radiat Oncol Biol Phys*. 2002;52:333-338.
10. Pirzkall A, Debus J, Lohr F, et al. Radiosurgery alone or in combination with whole-brain radiotherapy for brain metastases. *J Clin Oncol*. 1998;16:3563-3569.
11. Aoyama H, Shirato H, Onimaru R, et al. Hypo-fractionated stereotactic radiotherapy alone without whole brain irradiation for patients with solitary and oligo brain metastasis using non-invasive fixation of the skull. *Int J Radiat Oncol Biol Phys*. 2003;56:793-800.
12. Chidel MA, Suh JH, Reddy CA, Chao ST, Lundbeck MF, Barnett GH. Application of recursive partitioning analysis and evaluation of the use of whole brain radiation among patients treated with stereotactic radiosurgery for newly diagnosed brain metastases. *Int J Radiat Oncol Biol Phys*. 2000;47:993-999.
13. Shirato H, Takamura A, Tomita M, et al. Stereotactic irradiation without whole-brain irradiation for single brain metastasis. *Int J Radiat Oncol Biol Phys*. 1997;37:385-391.
14. Shaw E, Scott C, Souhami L, et al. Radiosurgery for the treatment of previously irradiated recurrent primary brain tumors and brain metastases: initial report of Radiation Therapy Oncology Group protocol (90-05). *Int J Radiat Oncol Biol Phys*. 1996;34:647-654.
15. Joseph J, Adler JR, Cox RS, Hancock SL. Linear accelerator-based stereotaxic radiosurgery for brain metastases: the influence of number of lesions on survival. *J Clin Oncol*. 1996;14:1085-1092.
16. Trotti A, Byhardt R, Stetz J, et al. Common Toxicity Criteria version 2.0: an improved reference for grading the acute effects of cancer treatment: impact on radiotherapy. *Int J Radiat Oncol Biol Phys*. 2000;47:13-47.
17. Gaspar L, Scott C, Rotman M, et al. Recursive partition analysis (RPA) of prognostic factors in three Radiation Therapy Oncology Group (RTOG) brain metastases trials. *Int J Radiat Oncol Biol Phys*. 1997;37:745-751.
18. Radiation Therapy Oncology Group. RTOG/EORTC late radiation morbidity scoring schema. http://www.rtog.org/members/toxicity/late.html. Accessed June 15, 1999.
19. Kaplan EL, Meier P. Nonparametric estimation from incomplete observations. *J Am Stat Assoc*. 1958;53:457-481.
20. Cox D. Regression models and life tables. *J R Stat Soc [Ser A]*. 1972;34:187-220.
21. Leksell L. The stereotaxic method and radiosurgery of the brain. *Acta Chir Scand*. 1951;102:316-319.
22. Patchell RA, Tibbs PA, Walsh JW, et al. A randomized trial of surgery in the treatment of single metastases to the brain. *N Engl J Med*. 1990;322:494-500.
23. Mintz AH, Kestle J, Rathbone MP, et al. A randomized trial to assess the efficacy of surgery in addition to radiotherapy in patients with single cerebral metastasis. *Cancer*. 1996;78:1470-1476.
24. Vecht CJ, Haaxma-Reiche H, Noordijk EM, et al. Treatment of single brain metastasis: radiotherapy alone or combined with neurosurgery. *Ann Neurol*. 1993;33:583-590.

> The only true hope for civilization—the conviction of the individual that his inner life can affect outward events and that, whether or not he does so, he is responsible for them.
> —Stephen Spender (1909-1995)

— 84 —

# Residual motion of lung tumors in end-of-inhale respiratory gated radiotherapy based on external surrogates

Ross I. Berbeco[a]
Department of Radiation Oncology, Dana-Farber/Brigham and Women's Cancer Center
and Harvard Medical School, Boston, Massachusetts 02115

Seiko Nishioka
Department of Radiology, NTT Hospital, Sapporo, Japan

Hiroki Shirato
Department of Radiation Medicine, Hokkaido University School of Medicine, Sapporo, Japan

Steve B. Jiang
Department of Radiation Oncology, Massachusetts General Hospital and Harvard Medical School, Boston,
Massachusetts 02114

It has been noted that some lung tumors exhibit large periodic motion due to respiration. To limit the amount of dose to healthy lung tissues, many clinics have begun gating radiotherapy treatment using externally placed surrogates. It has been observed by several institutions that the end-of-exhale (EOE) tumor position is more reproducible than other phases of the breathing cycle, so the gating window is often set there. From a treatment planning perspective, end-of-inhale (EOI) phase might be preferred for gating because the expanded lungs will further decrease the healthy tissue within the treatment field. We simulate gated treatment at the EOI phase, using a set of recently measured internal/external anatomy patient data. This paper attempts to answer three questions: (1) How much is the tumor residual motion when we use an external surrogate gating window at EOI? (2) How could we reduce the residual motion in the EOI gating window? (3) Is there a preference for amplitude- versus phase-based gating at EOI? We found that under free breathing conditions the residual motion of the tumors is much larger for EOI phase than for EOE phase. The mean values of residual motion at EOI were found to be 2.2 and 2.7 mm for amplitude- and phase-based gating, respectively, and, at EOE, 1.0 and 1.2 mm for amplitude- and phase-based gating, respectively. However, we note that the residual motion in the EOI gating window is correlated well with the reproducibility of the external surface position in the EOI phase. Using the results of a published breath-coaching study, we deduce that the residual motion of a lung tumor at EOI would approach that at EOE, with the same duty cycle (30%), under breath-coaching conditions. Additionally, we found that under these same conditions, phase-based gating approaches the same residual motion as amplitude-based gating, going from a 28% difference to 11%, for the patient with the largest difference between the two gating modalities. We conclude that it is feasible to achieve the same reproducibility of tumor location at EOI as at EOE if breath coaching is implemented, enabling us to reap the benefits of the dosimetric advantage of EOI gating. © 2006 American Association of Physicists in Medicine. [DOI: 10.1118/1.2358197]

Key words: radiotherapy, gating, residual motion, organ motion, breath coaching

## I. INTRODUCTION

In external beam radiotherapy, there is a dosimetric advantage to treating a lung patient at inspiration. To this end, clinics have used breath hold techniques such as deep-inspiration breath hold (DIBH) to reduce lung toxicity.[1–4] However, DIBH may not be suitable for lung cancer patients who have compromised pulmonary function.[4] For these patients, it may still be beneficial to use gated radiotherapy under normal breathing conditions (i.e., not deep-inspiration) at end-of-inhale (EOI), as opposed to end-of-exhale (EOE).

During normal breathing, total lung volume can increase by 12%–40% (mean: 22%) at inhalation.[5] Of course, the actual amount is highly patient dependent. A corollary to the increase in lung volume at inspiration is the decrease in physical density of the lung. Lung density is not only a function of breathing phase but also gender, age, and location (among other things). Compiling a set of categorical measurements of lung density at different breathing phases is difficult because of all of these factors. Fujisaki et al. found the average lung density at "shallow inspiration," "shallow expiration," and free-breathing to be 0.17, 0.23 g/cc, and 0.22 g/cc, respectively.[6] However, it is unclear how "shallow inspiration" is defined in that work.

A recent study by Biancia et al. has shown that there is a "minor" dosimetric benefit to gating at normal EOI (i.e., without a deep breath-hold maneuver) for the ten patients

studied.[5] In general, a treatment beam of the same aperture irradiates less healthy lung tissue with the patient at inhale than at exhale. Exactly how much is spared depends on the location of the tumor as well as age, gender, pulmonary ability, and other physiological patient-specific factors. Biancia *et al.* based their results on the lungs as the only limiting structure in dose escalation (dose to the spinal cord was calculated but not taken into account for dose escalation, the esophagus was not taken into account at all). They report that the average maximum prescription dose—with the constraint that NTCP $\leq$25%—is 89.6 Gy for EOE and 94 Gy for EOI.[5] However, half of the patients studied show an absolute difference in maximum prescription dose less than 3.5%, while the other half ranges from 8% to 15.6% (mean: 12.5%), all in favor of EOI gating.[7] For the five patients that showed a strong dosimetric benefit with EOI gating, the maximum prescription dose—with the constraint that NTCP $\leq$25%– is 76.6 Gy for EOE and 86.2 Gy for EOI. In a recently published, large population study, it was reported that 5 year local control rates increase approximately 1.3% for every 1 Gy delivered above 70 Gy ($R^2$=0.981).[8] From the results of that study, we can deduce that, on average, for the patients studied by Biancia *et al.*, the 5 year local control rates would increase from 44.5% to 50.1% if EOI gating were used instead of EOE. For the half of the patients that showed the most benefit from EOI gating, the 5 year local control rates would increase from 28.0% to 40.2%, with the greatest advantage for one patient being an increase of 29.8% to 45.1%. These numbers clearly show that the dosimetric benefit of EOI gating is patient dependent and the increase in local control versus EOE gating can be significant.

A drawback to EOI gating that has been noted in previous publications is that the amplitude of EOE is more reproducible than EOI.[4,9,10] This would seem to make EOE phase safer and less time consuming for clinical respiratory gating, although the irradiation occurs when the lungs are in their densest state. The present study was performed with the intention of determining whether the large external surrogate residual motion at EOI translates into large tumor residual motion, and, if so, whether abatement of the motion is possible by increasing the reproducibility of the external marker at EOI. We investigated the possibility of reducing the tumor residual motion at EOI to the level of EOE. Our goal is to explore a gating scheme that combines the dosimetric advantages of EOI irradiation with the better reproducibility of EOE.

This is not a treatment planning study. This is a study of the tumor position, not its geometry or the relative geometries of adjacent structures. Ideally, this investigation would include true four-dimensional volumetric data to analyze the delivered dose for an entire course of treatment, but that is not technically feasible at this time. Therefore, this inquiry is purely an analysis of the precision of a gating technique.
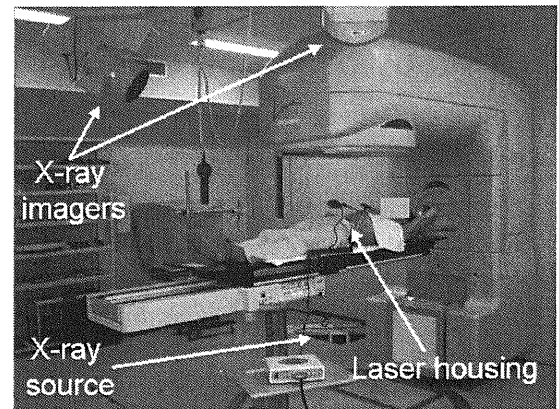
FIG. 1. The experimental setup is shown. the patient's abdomen is monitored by the RespGate system, a laser displacement device attached to the couch. The position of the internal gold bb is monitored by the stereoscopic fluoroscopy (only one x-ray source is visible in the picture). Note that for certain gantry angles, one of the x-ray imagers may be obscured.

## II. METHODS AND MATERIALS

### A. External and internal gating systems

The Radiation Oncology clinic at the Nippon Telegraph and Telephone Corporation (NTT) Hospital in Sapporo, Japan, is equipped with a Mitsubishi Real-time Radiation Therapy (RTRT) system.[11] Patients with abdominal and thoracic tumors, treated with this system, typically have two to four 1.5 mm diameter gold ball-bearings (bb's) implanted in or near the tumor.[12] During treatment, one of these radiopaque markers is tracked in real-time with stereoscopic diagnostic x-ray fluoroscopy, and the treatment beam is turned on when the marker is within a predetermined 3D window.[11] An external surrogate gating system was installed and integrated with the RTRT system by Mitsubishi (see Fig. 1). The AZ-733V "RespGate" external respiratory gating system (Anzai Medical, Tokyo, Japan) monitors the movement of the patient's abdominal surface by a laser displacement sensor. This gives a relative measurement of the distance from the laser housing to the abdomen. The signal from the surface monitor is synchronized with the signal from the fluoroscopic unit so that the log files contain the three-dimensional marker position and the external surface position at every time point [see Fig. 2(a) and 2(b)]. The rate of data acquisition for this entire system is 30 frames per second. Note that the fluoroscopic and laser measurements are taken even when the treatment beam is gated off. We are extracting continuous data while the treatment, itself, is gated. We use the internal/external correlated data to perform simulations of external gating scenarios (like the study presented here). The imaging is performed throughout each treatment, so we were able to obtain large statistics. This is the only dataset that has been published with synchronized 3D tumor location and 1D abdominal position for complete treatments of multiple lung patients.[13]
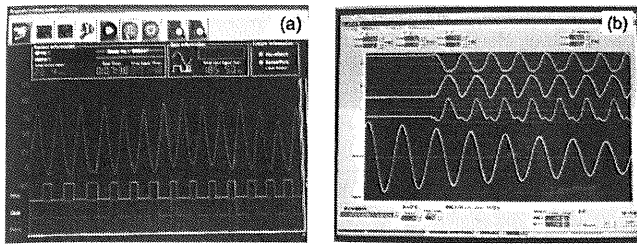
FIG. 2. (a) A screen capture of the output of the RespGate system is shown for a patient during treatment. For some gantry angles, the fluoroscopic view is blocked and the external system has to be used for treatment. Only angles for which both the RTRT and RespGate systems are not obscured were used in this study. (b) The output of the RTRT + RespGate system is shown for a QA phantom. The top three curves represent the position of the gold bb in the lateral, cranial-caudal, and anterior-posterior directions, respectively. The bottom curve is the output of the RespGate external gating system. For this QA phantom, the two signals are purposely decoupled and the external signal is a damped harmonic oscillation.

## B. The patients

A total of eight lung patients were studied. The details of each patient are given in Table I. Data were taken for only a single day for patients 1–3; because no radiotherapy treatment was given to these patients at the NTT hospital, they were brought in to test the feasibility of the system. Patients 4–8 were treated with 40–48 Gy in 4–8 fractions. All of patients in this analysis have internal marker motion greater than 1 cm peak-to-peak. Patient 5 was treated twice, 2 months apart. Since the same site was treated and no isocenter shift was made, we used both sets of data in the evaluation, under the same patient name. Some beams/days were excluded because the patient shifted during treatment.

In this study, the patients were not coached during their treatments. The resulting data are considered "free-breathing" and a good representation of how patients can change their breathing while on the treatment couch if they are not coached.

## C. Patient setup

In the CT simulation session, a scan is taken with the patient's breath held at EOE. At each treatment session, pa-

TABLE I. Information about the patients studied. Patient 5 was treated twice, at the same site, with 2 months between treatments. The tumor site is indicated using the common anatomical notation for lung segmentations: S1-3 is upper lobe, S4-5 is middle lobe, and S6-10 is lower lobe.

| Patient | Gender | Age | No. of bb's | Tumor site | Fractions |
|---------|--------|-----|-------------|------------|-----------|
| 1 | F | 47 | 4 | Rt.S7 | 1 |
| 2 | F | 70 | 3 | Lt.S6 | 1 |
| 3 | F | 71 | 2 | Rt.S5 | 1 |
| 4 | F | 47 | 3 | Rt.S4 | 8 |
| 5 | M | 81 | 3 | Rt.S2b | 4 |
| 5 | | | | | 8 |
| 6 | M | 61 | 3 | Rt.S10 | 8 |
| 7 | M | 68 | 3 | Rt.S6 | 4 |
| 8 | M | 85 | 3 | Rt.S8 | 4 |

tients are initially set up to skin marks using in-room lasers. Short fluoroscopic imaging sessions are performed to determine the position of the markers at the EOE phase. The 3D marker position is compared to the planned position. The RTRT system then calculates the appropriate couch shift (performed by the therapist) to bring the target to isocenter. The physician monitors the fluoroscopy to verify that the markers are properly tracked and can reach the internal gating window at EOE. This internal fiducial-based setup procedure eliminates the daily setup error (interfractional variations). Any positional errors occurring during the treatment are then due to intrafractional variations. This is a very important point: because the patient is setup based on the fiducial marker position (tumor-based setup versus bony anatomy-based setup) there is essentially no setup error. A complete description of the treatment procedure has been given by Shirato *et al.*[14]

## D. Data analysis

The data acquired by both the internal and external monitoring systems indicate a "position" at each time step. For the external monitoring system, position is the distance from the abdominal surface to the laser housing. In the internal monitoring system, the position of the tracked marker is calculated in isocenter coordinates. The internal marker position and external surface displacement are written to a logfile that is exported for off-line evaluation. To calculate the phase of the external signal for each time point, a retrospective algorithm is employed.[15] The EOI is assigned phase angle $0/2\pi$, and the phase angle of EOE is generally around $\pi$, depending on the shape of the breathing waveform. Assigning phase retrospectively allows us to avoid the issue of phase assignment in real-time, a necessary and very difficult calculation that is needed for clinical gating. Additionally, the analysis should not depend on the choice of algorithm for real-time phase calculation. The retrospective analysis ensures the best possible (if not clinically unachievable) phase assignation.

### 1. Amplitude-based gating

In this study, the external surrogate's amplitude-based gating window was chosen to encompass EOI. The gate is opened when the amplitude of the external monitoring system reaches the lower amplitude threshold, and closed when the amplitude falls back below the threshold. A gating window was chosen for each treatment beam such that the duty cycle was approximately 30% with the upper boundary greater than the maximum amplitude of the external surface during that treatment beam. The residual motion is defined to be the motion of internal markers during the open external gating window. For each beam, there is a 3D collection of data points representing the positions of the internal marker when the external amplitude was within the gating window. The median of these points (the median gated position) is the reference point from which the tumor residual motion $(r_{internal})$ is calculated. $r_{internal}$ is the magnitude of the 3D distance between each gated data point and the median gated position. This is the metric of tumor residual motion.

TABLE II. The mean and 95th percentile residual motion for amplitude- and phase-based gating at inhale and exhale, respectively, for a 30% duty cycle (A=amplitude-based gating, P=phase-based gating, n=negligible motion). The 95th percentile residual motion is the smallest amount of residual motion encompassing 95% of the date points (this can be thought of as the $2\sigma$ range).

| Patient | Total internal motion (mm) LR/SI/AP | Mean residual motion (mm) | | | | 95th percentile residual motion (mm) | | | |
|---|---|---|---|---|---|---|---|---|---|
| | | Inhale | | Exhale | | Inhale | | Exhale | |
| | | A | P | A | P | A | P | A | P |
| 1 | n/19/6 | 3.8 | 4.7 | 0.9 | 1.4 | 9.7 | 10.3 | 2.0 | 3.2 |
| 2 | n/13/n | 2.8 | 3.8 | 1.1 | 0.9 | 7.6 | 6.6 | 2.6 | 2.2 |
| 3 | 5/5/9 | 1.8 | 1.7 | 1.2 | 0.9 | 4.8 | 3.2 | 4.1 | 1.6 |
| 4 | n/10/6 | 1.4 | 1.5 | 0.7 | 0.7 | 3.0 | 3.0 | 1.8 | 1.4 |
| 5 | n/10/5 | 1.4 | 1.4 | 0.6 | 0.8 | 2.9 | 2.8 | 1.1 | 1.5 |
| 6 | n/12/n | 1.7 | 2.3 | 1.2 | 1.7 | 3.8 | 5.5 | 3.1 | 4.8 |
| 7 | n/10/n | 1.6 | 1.7 | 0.4 | 0.4 | 3.1 | 3.3 | 0.9 | 0.8 |
| 8 | n/15/6 | 3.2 | 4.3 | 1.9 | 2.8 | 6.7 | 9.3 | 3.7 | 6.0 |
| Average | n/12/n | 2.2 | 2.7 | 1.0 | 1.2 | 5.2 | 5.5 | 2.4 | 2.7 |

## 2. Phase-based gating

A similar analysis is performed for the external surrogate's phase-based gating window. The two phase values that define the boundaries of the gating window are found by an exhaustive search of all phase angle windows in 0.1 rad increments. The gate is selected that results in the lowest residual motion for 30% duty cycle with the requirement of including EOI. This represents the best possible phase gating region for EOI gating. The tumor residual motion is defined to be the collection of internal data points corresponding to the external gating window. The median of these points (the median gated position) is the reference point from which $r_{internal}$ is calculated, similar to the calculation of tumor residual motion for amplitude-based gating.

## III. RESULTS

## A. Inhale versus exhale gating

The results of the analysis described above are shown in Table II with the EOE-gated data for comparison.[13] Note that these two analyses (EOI and EOE) were conducted with the same (30%) duty cycle. Also shown is the total internal ungated tumor motion in all three directions (LR, SI, and AP). Even though gating at EOI decreases the tumor motion relative to continuous, ungated treatment, gating at EOE is clearly superior, in this respect. At least some increase in residual motion is seen for every patient when EOI gating is compared to EOE. Averaging the patients, EOI gating gives a mean residual motion of 2.2 and 2.7 mm for amplitude- and phase-based gating, respectively, while EOE gating gives 1.0 and 1.2 mm for the same quantities, respectively. In an alternative analysis of the data, we sought an EOI gate that would produce the same amount of residual motion as the EOE gate, and compared the duty cycles. These results are presented in Table III. For some patients, the EOE residual motion can never be reached with EOI gating. From both of

these analyses, we can see that, in the absence of any form of breath coaching, EOE gating is preferable to EOI gating. But how much of this advantage is due to external amplitude reproducibility and how much is due to actual internal/external correlation? In other words, if the external EOI position were reproducible for each breathing cycle, would the residual motion for EOI and EOE gating be equivalent?

We investigated this hypothesis by looking at the relationship between the mean residual motion and the normalized standard deviation of the external maxima, $\langle\sigma\rangle_{inhale}$, where

$$\langle\sigma\rangle_{inhale} = \frac{\sigma_{inhale}}{(1/N)\Sigma_i^N a_i}.$$

$\sigma_{inhale}$ is the standard deviation of the external maxima (end-of-inhale), $a_i$ is the peak-to-peak external amplitude of the $i$th breathing cycle, and $N$ is the total number of breathing cycles. The normalized standard deviation of the external minima, $\langle\sigma\rangle_{exhale}$, is similarly defined:

TABLE III. An alternative analysis. The duty cycles (%) for inhale gating that give a residual motion equivalent to exhale gating at 30% duty cycle. For some patients, the EOE residual motion can never be reached with EOI gating.

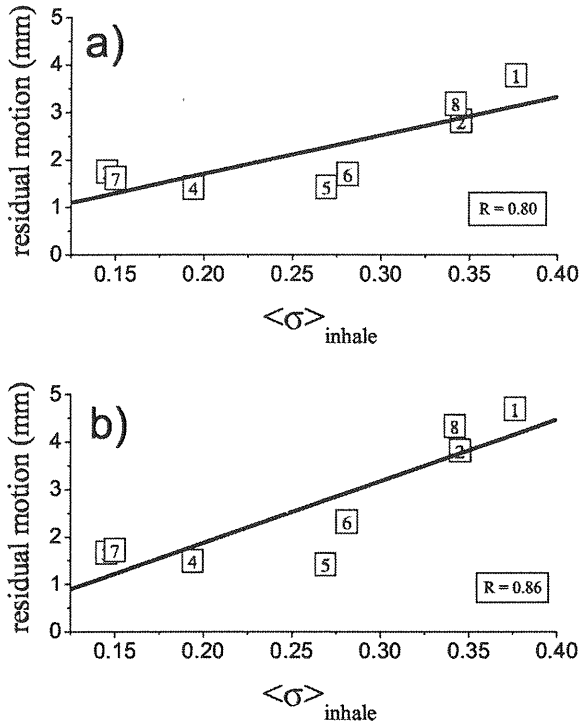| Patient | Inhale gating duty cycle | |
|---|---|---|
| | Amplitude-based | Phase-based |
| 1 | 2% | <1% |
| 2 | <1% | <1% |
| 3 | 20% | 3% |
| 4 | 2% | <1% |
| 5 | 1% | 2% |
| 6 | 15% | 22% |
| 7 | <1% | <1% |
| 8 | 1% | 7% |

FIG. 3. The mean residual motion is shown as a function of the normalized standard deviation of the external EOI position ($\langle\sigma\rangle_{inhale}$) for (a) amplitude-based and (b) phase-based gating. Each data point represents the mean over the entire treatment for each patient, respectively. The best-fit line is drawn and respective $R$-value shown.

$$\langle\sigma\rangle_{exhale} = \frac{\sigma_{exhale}}{(1/N)\Sigma_i^N a_i}.$$

Figure 3 shows that for amplitude- and phase-based gating, patients with more reproducible EOIs tend to exhibit less residual motion of their lung tumors. Figures 4(a) and 4(b) show the $\langle\sigma\rangle_{exhale}$ and $\langle\sigma\rangle_{inhale}$ for amplitude- and phase-based gating for patient 6, with each data point representing a single beam. When a patient's breathing is more reproducible, the residual motion at EOI decreases. This trend is true for all of the patients studied for both gating modalities. Fig. 4(c) is a combination of Figs. 4(a) and 4(b). As the reproducibility of the EOI position becomes similar to that for EOE, the residual motion converges. This means that the residual motion in EOI gating can approach that of EOE gating if the reproducibility of the external position is the same.

A proven method for improving the repeatability of the external signal is patient breath coaching.[16-18] Neicu *et al.* used audio/visual coaching in the form of a "breathe in"/ "breathe out" prompt and LCD goggles, showing the patients' breathing curve in near real-time. The authors of that study have shown that $\langle\sigma\rangle_{inhale}$ can be reduced from about 0.22 to 0.11 for free-breathing and audio-visual coaching, respectively.[18] In addition, $\langle\sigma\rangle_{exhale}$ can be reduced from 0.10 to 0.07, for free-breathing and audio-visual coaching, respectively. These are the averages among ten patients in a clinical setting. The reproducibility of the breath coached EOI posi-
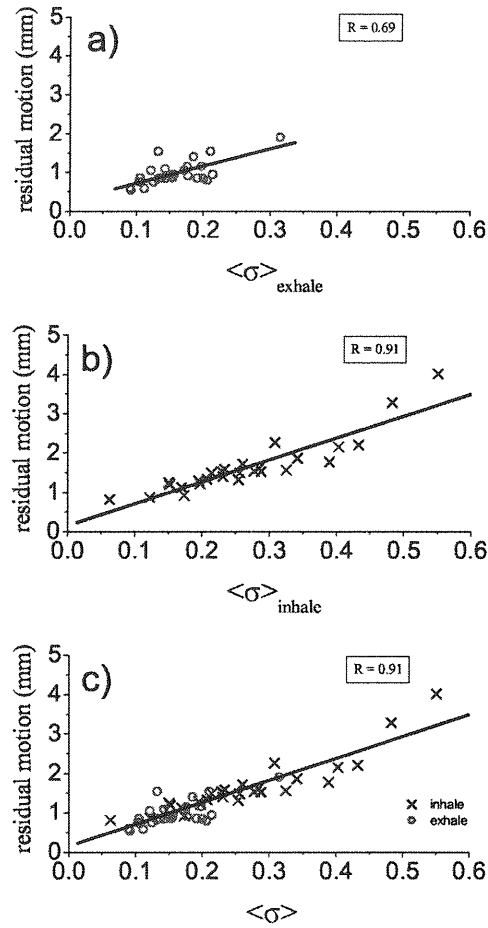


FIG. 4. The mean residual motion, for patient 6, is plotted as a function of the normalized standard deviation of the external (a) EOE amplitude and (b) EOI amplitude, for amplitude-based gating. The combination is shown in (c). The best-fit line is drawn and respective $R$ value shown.

tion approaches that of the free-breathing EOE position and, in half of the cases studied by Neicu *et al.*, is superior. Extending this result to our patients, we find that if $\langle\sigma\rangle_{inhale}$ approaches $\langle\sigma\rangle_{exhale}$, the residual motion of the lung tumors will be similar [as seen in Fig. 4(c)].

## B. Phase versus amplitude gating at EOI

Half of the patients (1, 2, 6, and 8) show less mean residual motion with amplitude-based gating than with phase-based gating, at EOI. The other half shows an insignificant difference ($<10\%$) between the two. The 95th percentile data show that two of the patients (2 and 3) have more significant tails for amplitude gating than phase gating. Otherwise, the data are consistent with the mean residual motion. Overall, the data indicate that an advantageous decrease in residual motion can be achieved by using amplitude-based gating rather than phase-based gating.

We studied the relationship between $\langle\sigma\rangle_{inhale}$ and the phase/amplitude-gating question. It was found that reducing $\langle\sigma\rangle_{inhale}$ tends to reduce the importance of which gating mode
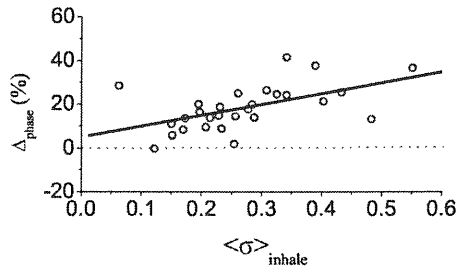
FIG. 5. $\Delta_{phase}$ is plotted as a function of the normalized standard deviation of the EOI external amplitude. the best-fit line is drawn to show the data trend; it should not be inferred that a linear relationship exists.

TABLE IV. The normalized standard deviation of beam-to-beam mean residual motion for amplitude- and phase-based gating at EOI and EOE.

| Patient | Inhale | | Exhale | |
|---|---|---|---|---|
| | Amplitude | Phase | Amplitude | Phase |
| 4 | 0.14 | 0.20 | 0.22 | 0.29 |
| 5 | 0.30 | 0.35 | 0.48 | 0.47 |
| 6 | 0.41 | 0.52 | 0.32 | 0.41 |
| 7 | 0.11 | 0.24 | 0.38 | 0.44 |
| 8 | 0.19 | 0.27 | 0.26 | 0.34 |

is selected. This is illustrated in Fig. 5. We define the relative percent difference between the mean residual motions due to amplitude- and phase-based gating to be

$$\Delta_{phase} = \frac{\bar{R}_{phase} - \bar{R}_{amplitude}}{\bar{R}_{phase}} \times 100,$$

where $\bar{R}_{phase}$ and $\bar{R}_{amplitude}$ are the mean residual motions due to phase- and amplitude-based gating, respectively. Among the multi-fraction patients, patient 6 has the largest $\Delta_{phase}$ ($\Delta_{phase}=26\%$). The results of Neicu *et al.* indicate that, with breath coaching, the mean $\langle\sigma\rangle_{inhale}$ could drop from 0.28 to 0.17. This new mean $\langle\sigma\rangle_{inhale}$ implies a mean $\Delta_{phase}$ of 11%, indicating that amplitude is still better than phase, but by a much smaller margin.

## C. Variation in residual motion

We studied the variability of the residual motion, beam-to-beam and day-to-day, throughout the course of treatment. For this part of the study, the first three patients were not
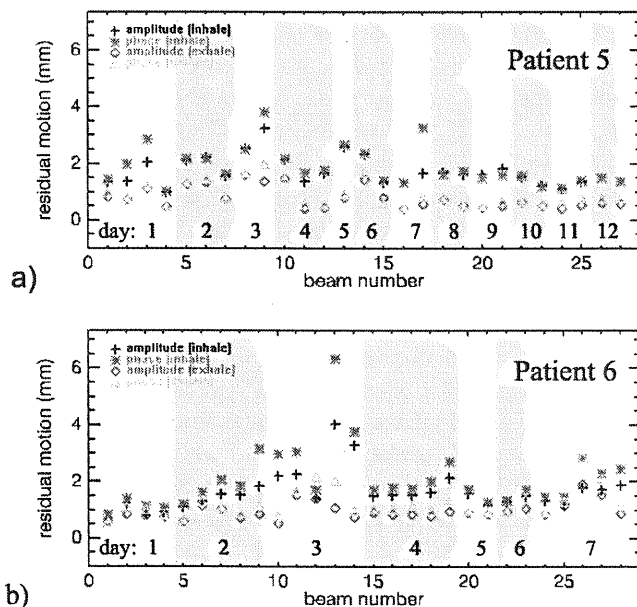




FIG. 6. (a) and (b) The mean residual motion is shown as a function of beam and day for patients 5 and 6, respectively. Shown are the results for amplitude- and phase-based gating at EOI and EOE.

analyzed. The mean residual motion as a function of beam and as a function of day, for patients 5 and 6 are shown in Fig. 6. Results are shown for amplitude- and phase-based gating at EOE and EOI. Patient 5 exhibited considerable variation in all modalities at the beginning of treatment, but settled down when he returned for his second course of treatment (days 5–12). Also, the residual motion showed an overall decline throughout the treatment. Patient 6 began with low, consistent residual motion on day 1. It became worse with extreme variation and high residual motion peaking on day 3 before returning to a more constant situation. Overall, EOE gating has systematically less residual motion than EOI for every patient throughout the treatment, in the absence of breath coaching.

Table IV shows the normalized standard deviation of mean residual motion from beam-to-beam for patients 4–8. Here, normalized standard deviation of mean residual motion is

$$\sigma_{beam} = \frac{\sqrt{(1/N)\Sigma_{i=1}^{N}(r_i - (1/N)\Sigma_{i=1}^{N}r_i)^2}}{(1/N)\Sigma_{i=1}^{N}r_i},$$

where $r_i$ is the mean $r_{internal}$ for beam $i$ and $N$ is the total number of beams. With the exception of patient 6, $\sigma_{beam}$ is less for EOI gating than EOE. For all patients, $\sigma_{beam}$ for amplitude-based gating is less than or approximately equal to phase-based gating. The least amount of beam-to-beam variation can therefore be found in amplitude gating and EOI (except for patient 6, who shows the least amount of variation for amplitude gating at EOE). Table V, shows the same analysis on a day-to-day basis. Similar results are found, with the least daily variation for amplitude gating at EOI (with the exception of patient 6). At this time, we can offer

TABLE V. The normalized standard deviation of daily mean residual motion for amplitude- and phase-based gating at EOI and EOE.

| Patient | Inhale | | Exhale | |
|---|---|---|---|---|
| | Amplitude | Phase | Amplitude | Phase |
| 4 | 0.11 | 0.13 | 0.18 | 0.20 |
| 5 | 0.28 | 0.29 | 0.41 | 0.39 |
| 6 | 0.32 | 0.40 | 0.17 | 0.25 |
| 7 | 0.13 | 0.15 | 0.39 | 0.45 |
| 8 | 0.07 | 0.11 | 0.12 | 0.24 |

no explanation for why patient 6 behaves differently. Overall, the change in residual motion for EOI is on roughly the same scale as EOE. That is to say that there can be great changes on the scale of minutes, hours, and days. This varies by patient, but it is unclear how one would predict which patients will have the most/least variability throughout treatment.

## IV. DISCUSSION

The residual motion of lung tumors has been studied in eight patients for a hypothetical, externally defined EOI gated treatment. It was found that amplitude-based gating is superior to phase-based gating, but that the difference can be diminished under breath coaching conditions. However, these results were found with the phase computed in an ideal manner (retrospective phase definition and optimized gating window). In general, the phase gating will be worse than this, so amplitude gating may be preferable in a clinical setting. This will be investigated further in future studies. The results were also compared to a previous study, with the same patients, of EOE gated treatment.[13] Upon first inspection, it was found that the latter method produced much less residual motion within the gating window than the former (EOI). However, taking EOI position reproducibility into account, we deduce that the residual motion of breath coached EOI gating will be equivalent to the residual motion of EOE gating. Our deduction is based on the combination of two different experiments. To definitively prove the point, the experiment in Sapporo should be repeated with breath coaching. Still, based on our results, we believe that EOI gating is clinically feasible as long as proper margins are employed and breath coaching is performed. Please note that the breath coaching should also be employed during 4DCT acquisition to ensure consistency. We would also like to point out that, in principle, patients could be coached to fuller than normal inspiration to expand the dosimetric advantage of inhale gating.

The variation in mean residual motion can be large from beam-to-beam and day-to-day. Also, the mean residual motion can increase or decrease throughout the course of treatment. There appears to be no external warning of when the residual motion might increase/decrease. Margins accounting for residual motion should be carefully defined. Tight gating margins based on a single simulation session at the beginning of the course of treatment may not represent the true tumor residual motion as the treatment progresses [see Figs. 6(a) and 6(b)]. Correct residual motion margin calculation can be studied further with this data.

In our previous study of EOE gating, we expressed our opinion that when gating is based on an external surrogate, some method of verification should be employed *during* the treatment, to ensure that the tumor is being targeted correctly. We repeat that caveat here. The reduction in EOI residual motion to levels similar to EOE is a good first step towards EOI gating, but to confidently gate at any breathing phase, accurate tumor localization needs to be employed

throughout the treatment. This is a problem that we are currently studying.[19,20]

## V. CONCLUSIONS

Respiratory gating at EOI is a clinical option that may be preferable for some patients. The feasibility of producing acceptable tumor residual motion with breath coaching has been shown in this study. Problems due to irreproducibility of the inhale position can be alleviated by the introduction of a biofeedback breath-coaching procedure. We have shown that a reproducible external motion is well correlated with a reproducible internal one. We deduce that under breath-coaching conditions, gating at EOI should produce similar residual motion as EOE, for the same duty cycle.

## ACKNOWLEDGMENTS

[a]Electronic mail: rberbeco@lroc.harvard.edu

[1] J. Hanley *et al.*, "Deep inspiration breath-hold technique for lung tumors: the potential value of target immobilization and reduced lung density in dose escalation," Int. J. Radiat. Oncol., Biol., Phys. 45(3), 603–611 (1999).

[2] K. E. Rosenzweig *et al.*, "The deep inspiration breath-hold technique in the treatment of inoperable non-small-cell lung cancer," Int. J. Radiat. Oncol., Biol., Phys. 48(1), 81–87 (2000).

[3] E. D. Yorke *et al.*, "Evaluation of deep inspiration breath-hold lung treatment plans with Monte Carlo dose calculation," Int. J. Radiat. Oncol., Biol., Phys. 53(4), 1058–1070 (2002).

[4] G. S. Mageras and E. Yorke, "Deep inspiration breath hold and respiratory gating strategies for reducing organ motion in radiation treatment," Semin. Radiat. Oncol. 14(1), 65–75 (2004).

[5] C. D. Biancia *et al.*, "Comparison of end normal inspiration and expiration for gated intensity modulated radiation therapy (IMRT) of lung cancer," Radiother. Oncol. 75(2), 149–156 (2005).

[6] T. Fujisaki *et al.*, "Effects of density changes in the chest on lung stereotactic radiotherapy," Radiat. Med. 22(4), 233–238 (2004).

[7] C. D. Biancia, personal communication (2006).

[8] F. M. Kong *et al.*, "High-dose radiation improved local tumor control and overall survival in patients with inoperable/unresectable non-small-cell lung cancer: long-term results of a radiation dose escalation study," Int. J. Radiat. Oncol., Biol., Phys. 63(2), 324–333 (2005).

[9] Y. Seppenwoolde *et al.*, "Precise and real-time measurement of 3D tumor motion in lung due to breathing and heartbeat, measured during radiotherapy," Int. J. Radiat. Oncol., Biol., Phys. 53(4), 822–834 (2002).

[10] T. Kimura *et al.*, "Reproducibility of organ position using voluntary breath-hold method with spirometer for extracranial stereotactic radiotherapy," Int. J. Radiat. Oncol., Biol., Phys. 60(4), 1307–1313 (2004).

[11] H. Shirato *et al.*, "Physical aspects of a real-time tumor-tracking system for gated radiotherapy," Int. J. Radiat. Oncol., Biol., Phys. 48(4), 1187–1195 (2000).

[12] H. Shirato *et al.*, "Feasibility of insertion/implantation of 2.0-mm-diameter gold internal fiducial markers for precise setup and real-time tumor tracking in radiotherapy," Int. J. Radiat. Oncol., Biol., Phys. 56(1), 240–247 (2003).

[13] R. I. Berbeco *et al.*, "Residual motion of lung tumours in gated radiotherapy with external respiratory surrogates," Phys. Med. Biol. 50(16), 3655–3667 (2005).

[14] H. Shirato *et al.*, "Four-dimensional treatment planning and fluoroscopic real-time tumor tracking radiotherapy for moving tumor," Int. J. Radiat. Oncol., Biol., Phys. 48(2), 435–442 (2000).

[15] T. Neicu *et al.*, "Synchronized moving aperture radiation therapy

(SMART): average tumour trajectory for lung patients," Phys. Med. Biol. **48**(5), 587–598 (2003).

[16]V. R. Kini *et al.*, "Patient training in respiratory-gated radiotherapy," Med. Dosim **28**(1), 7–11 (2003).

[17]S. S. Vedam *et al.*, "Quantifying the predictability of diaphragm motion during respiration with a noninvasive external marker," Med. Phys. **30**(4), 505–513 (2003).

[18]T. Neicu *et al.*, "Synchronized moving aperture radiation therapy (SMART): improvement of breathing pattern reproducibility using respiratory coaching," Phys. Med. Biol. **51**(3), 617–636 (2006).

[19]R. I. Berbeco *et al.*, "A technique for respiratory-gated radiotherapy treatment verification with an EPID in cine mode," Phys. Med. Biol. **50**(16), 3669–3679 (2005).

[20]R. I. Berbeco *et al.*, "Towards fluoroscopic respiratory gating for lung tumours without radiopaque markers," Phys. Med. Biol. **50**(19), 4481–4490 (2005).

— 92 —

**CLINICAL INVESTIGATION**                                                                                   **Normal Tissues**

# THE UTILITY OF 18F-FLUORODEOXYGLUCOSE POSITRON EMISSION TOMOGRAPHY FOR EARLY DIAGNOSIS OF RADIATION-INDUCED MYOCARDIAL DAMAGE

KEIICHI JINGU, M.D.,* TOMOHIRO KANETA, M.D.,[†] KENJI NEMOTO, M.D.,* AZUSA ICHINOSE, M.D.,[†]
MINAKO OIKAWA, M.D.,[‡] YOSHIHIRO TAKAI, M.D.,* YOSHIHIRO OGAWA, M.D.,*
EIKO NAKATA, PH.D.,* TORU SAKAYAUCHI, M.D.,* KENJI TAKAI, M.D.,*
TOSHIYUKI SUGAWARA, M.D.,* KAKUTARO NARAZAKI, M.D.,* HIROSHI FUKUDA, M.D.,[§]
SHOKI TAKAHASHI, M.D.,[†] AND SHOGO YAMADA, M.D.*

Departments of *Therapeutic Radiology, [†]Diagnostic Radiology, and [‡]Cardiovascular Internal Medicine, Tohoku University School
of Medicine; and [§]Department of Nuclear Medicine and Radiology, Division of Brain Science, Institute of Development,
Aging, and Cancer, Tohoku University, Sendai, Japan

Purpose: We evaluated the clinical significance of focal increased uptake in the basal myocardium on F-fluorode-oxyglucose positron emission tomography (FDG-PET) in patients with esophageal cancer after radiotherapy.
Methods and Materials: Between August 2004 and July 2005, a total of 64 patients who had been irradiated for thoracic esophageal cancer underwent FDG-PET at least three months after the completion of chemoradiotherapy. Some patients showed increased FDG uptake in the basal portion of the myocardium. To clarify the clinical significance of these findings, further examinations of hearts were performed. The dose distribution in the myocardium with high FDG uptake was also analyzed retrospectively.
Results: Thirteen (20.3%) of the 64 patients showed high FDG uptake in the basal myocardium corresponding to the irradiated fields compared with FDG uptake in the myocardium outside the irradiated fields. Eight of the 13 patients consented to undergo examinations of the heart. Five of those eight patients showed low 123I-BMIPP uptake and four showed low 201TlCl uptake in the myocardium corresponding with high FDG uptake regions. In two patients, delayed enhancement was found in some parts of the area with high FDG uptake on Gd-DTPA magnetic resonance imaging (MRI), and the delay-enhanced lesion showed hypokinesia on cine-MRI in one patient.
Conclusions: FDG-PET often shows focal increased uptake in the basal myocardium after radiotherapy for esophageal cancer. This finding indicates the possibility of radiation-induced cardiac damage, and cardiac function and symptoms of such patients should be followed carefully. © 2006 Elsevier Inc.

Radiation-induced cardiomyopathy, Radiotherapy, FDG-PET, Delayed contrast MRI, Myocardial SPECT.

## INTRODUCTION

Positron emission tomography (PET) using 18F-fluorode-oxyglucose (FDG) is considered to be useful for evaluating tumor extension or detecting recurrence in patients with esophageal cancer. Therefore, FDG-PET is a promising noninvasive method for follow-up after chemoradiotherapy for esophageal cancer. Some patients have shown focal increased FDG uptake in the basal myocardium after completion of chemoradiotherapy. We suspected that these findings indicate myocardial damage induced by radiotherapy.

Before the 1960s, the myocardium was considered to be a relatively radiation-resistant organ, although pericardial effusion without symptoms after irradiation for the medias-

tinum often occurred. Recently, however, there have been many reports of patients with radiation-induced myocardial damage in the late phase (1–16). There have also been reports of occasional heart-related deaths in patients with esophageal cancer after radiotherapy (17, 18). Significant impairment of the left ventricular ejection fraction after radiotherapy for the mediastinum has also been reported (19). In addition, ischemic changes in the irradiated myocardium have been observed in some studies on myocardial perfusion imaging (7–9).

In the present study, we evaluated patients who showed focal increased FDG uptake in the basal myocardium after radiotherapy for esophageal cancer. To our knowledge, although we reported a case of radiation-induced cardiomy-

845

Table 1. Characteristics of all patients in the present study

| Characteristics of 64 patients | |
| --- | --- |
| Gender | Number of patients |
| Male | 60 |
| Female | 4 |
| Age | Years |
| Median | 66 |
| Range | 45–86 |
| Abnormal FDG accumulation | Number of patients |
| + | 13 |
| − | 51 |
| Stage UICC 1997 | Number of patients |
| 0-I | 20 |
| IIA-IIB | 12 |
| III | 20 |
| IVA-IVB | 6 |
| Postop | 6 |
| Total prescription dose | Gy |
| Median | 60 |
| Range | 30–70 |
| Concurrent chemotherapy | Number of patients |
| + | 51 |
| − | 13 |
| Site of primary tumor | Number of patients |
| Ut | 7 |
| Mt | 38 |
| Lt | 13 |
| Postop | 6 |
| Diabetes | Number of patients |
| + | 7 |
| − | 57 |
| History of myocardial infarction | Number of patients |
| + | 11 |
| − | 53 |

*Abbreviations:* UICC = Union Internationale Contre le Cancer; Ut = upper thoracic portion; Mt = midthoracic portion; Lt = lower thoracic portion.

opathy (20), there are no other reports of those FDG-PET findings that suggest radiation-induced myocardial damage. To clarify the clinical significance of these findings, we investigated the relationship with dose distribution in the myocardium and compared the findings of heart ultrasound (US), magnetic resonance imaging (MRI), and myocardial single-photon emission computed tomography (SPECT).

## METHODS AND MATERIALS

### Patients

Between August 2004 and July 2005, a total 64 patients (60 males and 4 females; median age, 66 years; range, 45 to 86 years) were enrolled in the present study with follow-up study for cancer. All patients had primary or postoperative recurrent thoracic esophageal cancer and had undergone irradiation to the mediastinum in our institution. Sixty-three patients had been proven to have squamous cell carcinoma, and one patient had been proven to have adenocarcinoma. The characteristics of all patients are shown in Table 1. Fifty-one patients were irradiated with concurrent chemotherapy. A combination of cisplatin or nedaplatin and 5-fluorouracil was used in 50 of those 51 patients, and TS-1 alone was used in one patient.

Our study was reviewed and approved by the Tohoku University Hospital Institutional Review Board and all patients gave informed consent.

### Radiotherapy

We mainly used 10 MV photons from a linear accelerator. The daily fractional dose of radiotherapy was 2.0 Gy, administered 5 days a week. Irradiation was performed using anterior-posterior opposing fields until about 40 Gy, and then using oblique opposing fields to avoid the spinal cord. Total irradiated prescription dose for the center of gross target volume ranged from 30–70 Gy (median, 60 Gy). Esophagectomy was performed in one patient because the tumor showed no change at a total irradiated dose of 30 Gy. The target volume was localized for radiotherapy in all patients by CT planning. Dose distribution was calculated by CADPLAN or ECLIPSE Varian Medical Systems (Palo Alto, CA) with Batho power law correction. Dose distribution in the myocardium with increased FDG uptake was analyzed retrospectively.

### PET

All patients underwent FDG-PET at a median of 9.25 months (range, 3 to 105 months) after the completion of radiotherapy. PET scans were performed 1 h after the administration of $^{18}$F-fluorodeoxyglucose at a dose of 3.1 MBq/kg using a Biograph PET/CT scanner or ECAT EXACT HR$^+$ PET scanner (Siemens, Hoffman Estates, IL) under the condition of more than four hours of fasting. Emission scans were performed for 2 min per position. Attenuation corrections were also performed. For semiquantitative analysis of increased FDG uptake lesions and normal myocardium, the maximal standard uptake value (SUV) based on body weight (g) was calculated and converted into a value-based lean body mass:
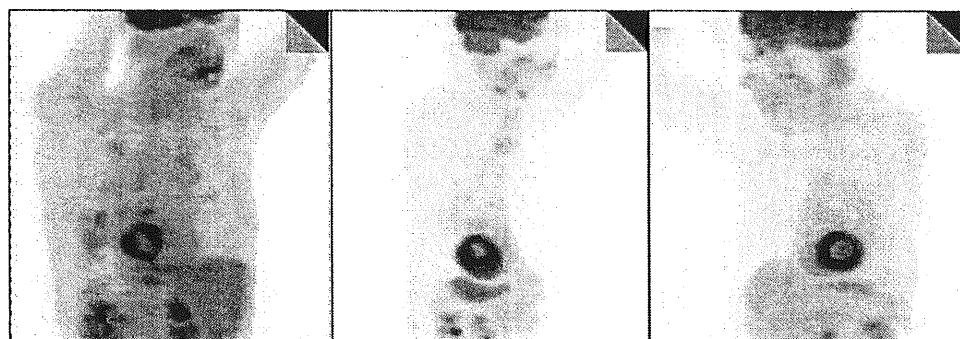


Fig. 1. Maximum intensity projection (MIP) image (Patients 2, 4, and 7). These are MIP images of three patients who had focal increased F-fluorodeoxyglucose uptake in the base of the myocardium, and the finding often looks like a ring.
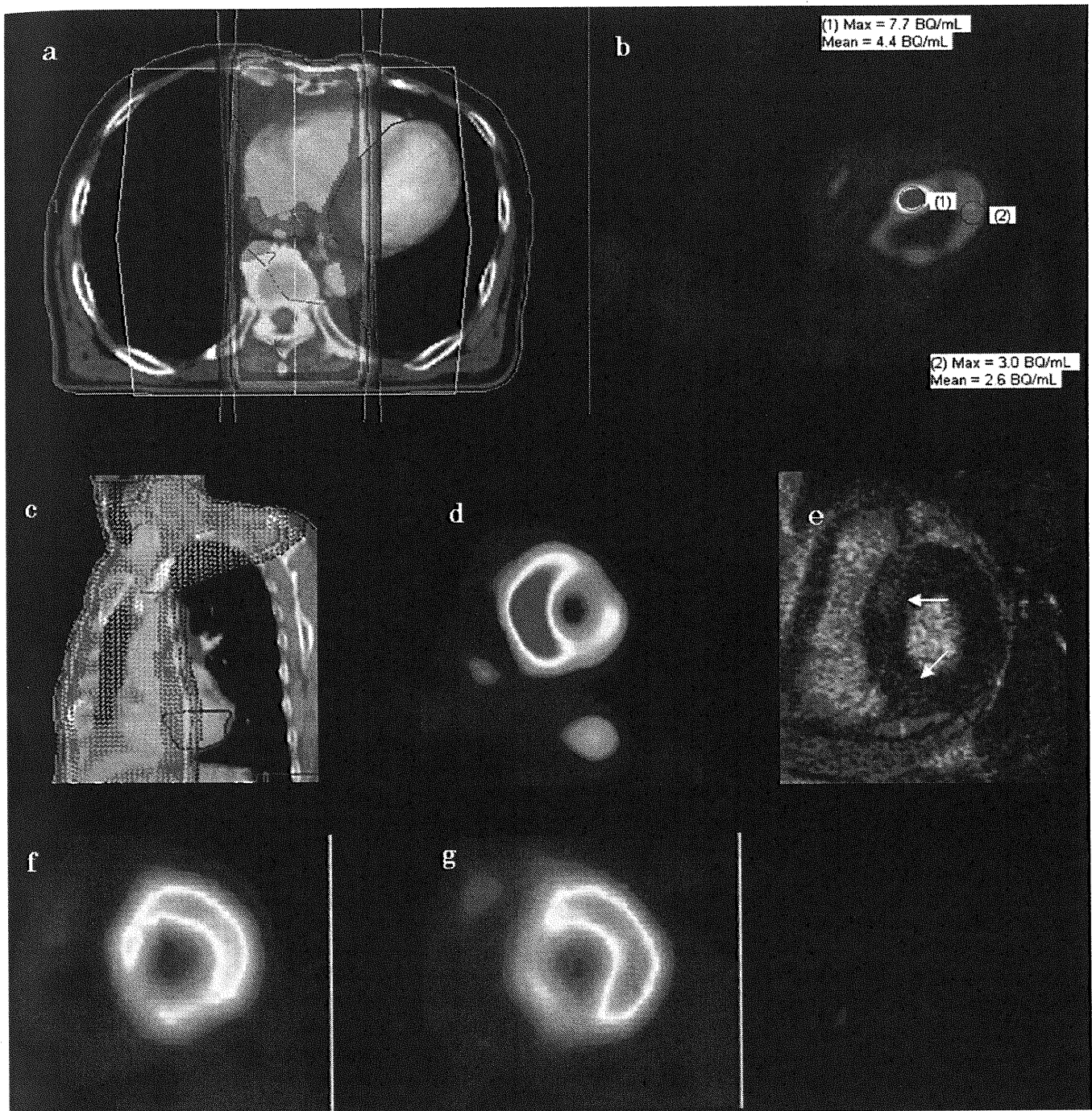
Fig. 2. Images of Patient 2 (68-year-old male) at six months after chemoradiotherapy for esophageal cancer (T1N0M0). (a) Dose-distribution axial image. (b) F-fluorodeoxyglucose-positron emission tomography (FDG-PET) axial image. (c) Dose-distribution short-axis image. (d) FDG-PET short-axis image. (e) gadolinium-magnetic resonance image (Gd-MRI) in delay phase. (f) $^{201}$TlCl short-axis image. (g) $^{123}$I-BMIPP short-axis image. FDG-PET clearly shows high FDG accumulation in the base of the left ventricular myocardium corresponding to the irradiated field. Gd-MRI shows slight enhancement in the base of the septum (arrows). $^{201}$TlCl and $^{123}$I-BMIPP uptake are decreased markedly in the lesion.

$$SUV = \text{tissue activity concentration } (Bq/mL)/$$

$$[\text{administered activity } (Bq)/\text{weight } (g)] \quad (1)$$

Cases with higher FDG uptake in the myocardium corresponding to the irradiated field than in other areas were diagnosed as positive findings with agreement of more than two nuclear medicine physi-cians. Patients with such positive findings who did not require additional therapy for recurrence and gave informed consent for enrollment in our study underwent further examinations of the heart by US, MRI, and myocardial SPECT. To investigate the state of metabolism and vascular flow in the myocardium, those patients underwent fatty acid metabolic SPECT and/or myocardial perfusion SPECT.
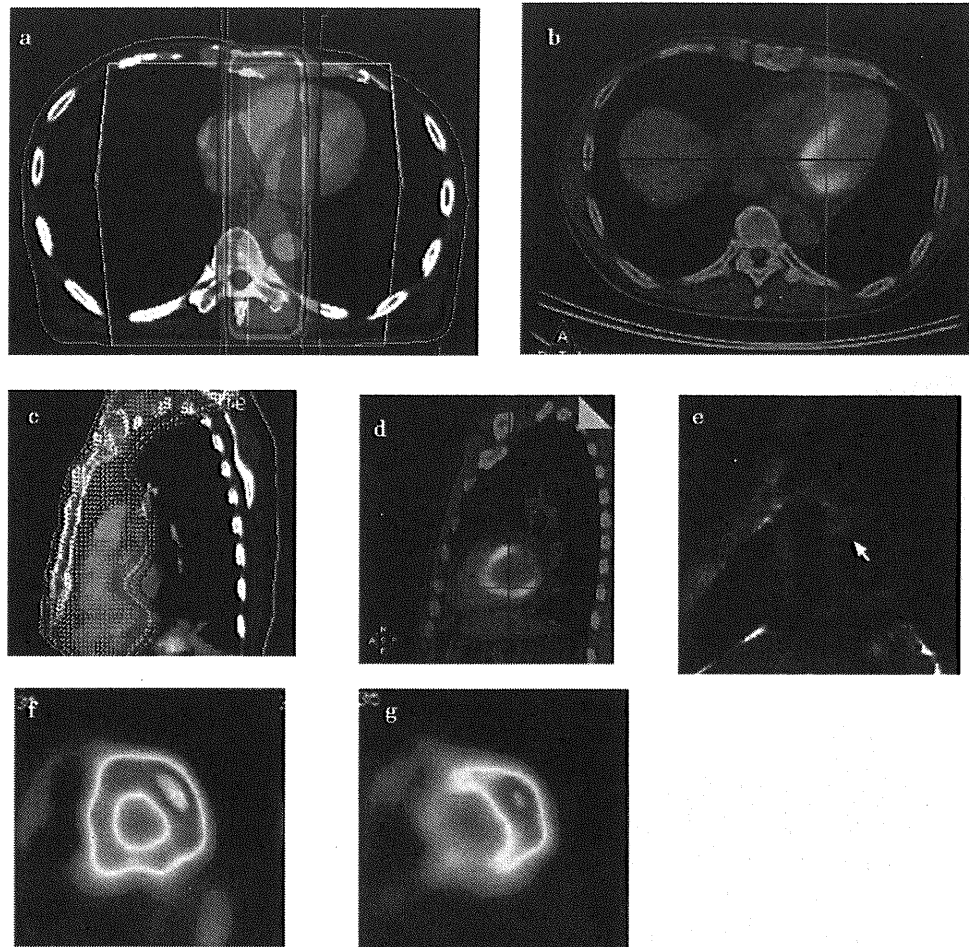
Fig. 3. Images of Patient 4 (55-year-old male) at five months after chemoradiotherapy for esophageal cancer (T4N1M1b). (a) Dose-distribution axial image. (b) F-fluorodeoxyglucose-positron emission tomography/computed tomography (FDG-PET/CT) axial image. (c) Dose-distribution short-axis image. (d) FDG-PET short-axis image. (e) Fatsat T2WI magnetic resonance imaging (MRI). (f) $^{201}$TlCl short-axis image. (g) $^{123}$I-BMIPP short-axis image. FDG-PET/CT clearly shows increased FDG uptake in the myocardium corresponding to the irradiated field. Fatsat T2WI MRI shows slight high signal in the base of the septum (arrows) without delayed-enhancement. $^{123}$I-BMIPP uptake is decreased markedly in the lesion, although $^{201}$TlCl uptake is normal.

*MRI*

Electrocardiogram-gated MRI was performed in breath-hold with a 1.5-T imager (Magnetom Vision, Siemens, Erlangen, Germany) using a body-array coil. Cine-MRI of the left ventricle in one horizontal, one vertical-long, and five short axial slices was performed using a gradient echo sequence (turbo FLASH) to evaluate the left ventricular anatomy and function. Five short-axial slices with 14-mm intervals were set from 1 cm below the level of the mitral-valve insertion to the apex. The acquisition parameters were as follows: Time to repeat/Time to echo (TR/TE) = 80/6.1 ms; flip angle, 25°; field of view (FOV), 300 mm, matrix, 182 × 256; thickness, 5 mm. Delayed contrast MRI in the same slice levels as those used for the cine-imaging was performed 15 min after injection of gadolinium-DTPA (0.1 mmol/kg) with a segmented inversion recovery gradient-echo pulse sequence. The acquisition parameters were as follows: TR/TE = 250/3.4 ms; flip angle, 15°; FOV, 300 mm; matrix, 220 × 256; thickness, 6 mm. The inversion time was adjusted to null normal myocardium (200–300 ms).

*SPECT*

Myocardial SPECT scans using thallium-201 ($^{201}$TlCl) and I-123 -methyl-iodophenyl pentadecanoic acid ($^{123}$I-BMIPP) were performed using a dual-detector gamma camera (MultiSPECT3, Siemens, Hoffman Estates, IL) with a low-energy, high-resolution collimator. $^{123}$I-BMIPP (111 MBq) and $^{201}$TlCl (74 MBq) were injected intravenously at the same time. At 30 min after the injection, SPECT scans were performed using two energy windows of the 159 keV photopeak of $^{123}$I with a 20% window and the 75 keV photopeak of $^{201}$Tl with a 20% window. No downscatter correction was performed.

## RESULTS

In the present study, 13 (20.3%) of the 64 patients showed high FDG uptake in the base of the left ventricular myocardium corresponding to the irradiated fields in comparison with FDG uptake in the myocardium outside the irradiated fields. The distribution of high FDG uptake is
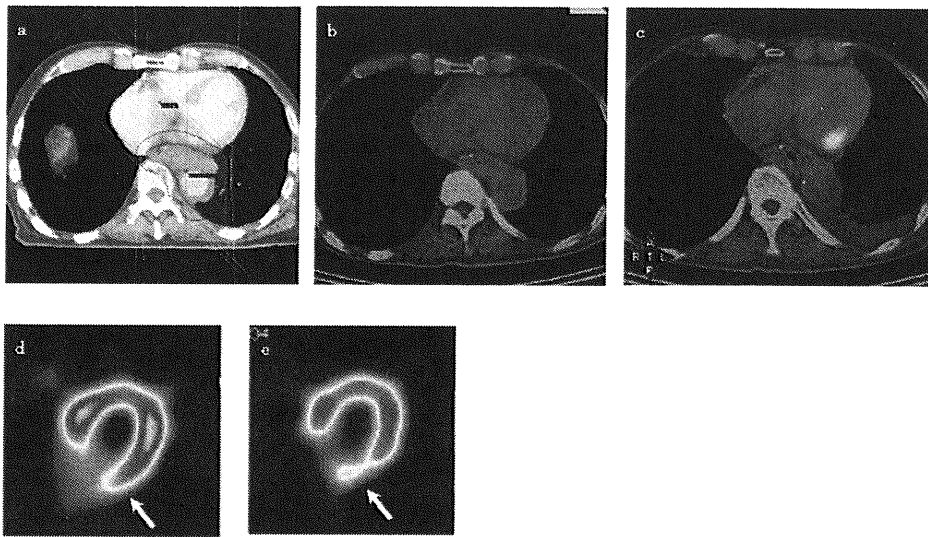
Fig. 4. Images of Patient 7 (78-year-old male) after chemoradiotherapy for postoperative recurrent esophageal cancer. (a) Dose-distribution axial image. (b) F-fluorodeoxyglucose-positron emission tomography/computed tomography (FDG-PET/CT) axial image one month after chemoradiotherapy. (c) FDG-PET/CT axial image five months after chemoradiotherapy. (d) $^{123}$I-BMIPP axial image. (e) $^{201}$TlCl axial image. FDG-PET/CT did not show abnormal FDG accumulation at one month after chemoradiotherapy but clearly showed high FDG accumulation in the high-dose irradiated myocardium at five months after chemoradiotherapy. $^{123}$I-BMIPP and $^{201}$TlCl uptake are decreased markedly in the region (arrows).

very characteristic and not consistent with the vascular territory of coronal arteries. That is, the high FDG uptake was seen in the basal portions of the anterior wall, posterior wall, lateral wall, and interventricular septum. This often looks like a ring in a maximum intensity projection image (Fig. 1).

The median SUV (max) values in the myocardium inside and that outside the irradiated fields of those 13 patients were 4.5 (range, 3.8 to 7.9) and 2.5 (range, 1.2 to 3.3), respectively. Eight of the 13 patients underwent cardiac examinations using SPECT and MRI. Five of those eight patients showed low $^{123}$I-BMIPP accumulation and four patients showed low $^{201}$TlCl accumulation in the base of the left ventricular myocardium, which matched exactly with the regions of high FDG accumulation (Figs. 2 through 4).

In two patients, delayed-contrast MRI showed delayed enhancement in some parts of the region with high FDG accumulation (Fig. 2). In one patient, a high signal on T2WI MRI was found in a part of the region with high FDG accumulation, but delayed enhancement was not significant (Fig. 3).

Characteristics of and results for these eight patients are shown in Table 2.

The median total irradiated dose in regions with high FDG accumulation was about 60 Gy (range, 40 to 70 Gy).

Few abnormalities of heart wall motion or left ventricular ejection fraction (LVEF) were detected by US in those patients. LVEF of those eight patients ranged from 0.43 to 0.87 (only patient 6 showed lower LVEF). No remarkable abnormalities were detected by US in the regions with high FDG uptake in any of the patients.

Abnormal FDG accumulation in the irradiated myocardium

was not significantly correlated with age, gender, stage, months after radiotherapy, site of primary tumor, diabetes, history of myocardial infarction, or concurrent chemotherapy.

## DISCUSSION

In the present study, 13 (20.3%) of the 64 patients who underwent irradiation for esophageal cancer showed high FDG uptake in the basal myocardium. The regions of high FDG uptake corresponded to the irradiated field but not to any coronary artery vascular territories. It is unlikely that these findings are a result of regional ischemia due to stenosis or occlusion of coronary arteries. Therefore, in this study, we explored the possibility of myocardial damage induced by radiation.

Myocardial SPECT studies were performed in eight patients, and six of those patients showed decreased uptake of $^{123}$I-BMIPP and/or $^{201}$TlCl in accordance with the focal high FDG uptake area. These facts suggest that radiation to the myocardium caused microvascular damage and impairment in myocardial perfusion and/or fatty acid metabolism. The findings of increased FDG uptake are consistent with these findings. It is known that the main energy source of the myocardium changes under the ischemic conditions. In a fasting state, the main energy source is thought to be free fatty acid, but the main energy source switches to glucose and lactate under ischemic conditions. Lauk et al. showed that radiation-induced microvascular damage to the myocardium occurred as a result of the direct effects of radiation on endothelial cells of capillaries of <0.2 mm in diameter within the myocardium, causing capillary swelling and progressive obstruction of the vessel lumen, leading to pericar-

Table 2. Characteristics of patients with high FDG accumulation in the myocardium in the irradiated field

| Patient | Total prescription dose (Gy) | Months after radiotherapy | $^{201}$TlCl | $^{123}$I-BMIPP | Gd-MRI | Symptom | Diabetes | History of myocardial infarction | Concurrent chemotherapy | LVEF |
|---|---|---|---|---|---|---|---|---|---|---|
| 1 | 64 | 5 | Normal | Normal | Normal | None | – | – | + | 0.69 |
| 2 | 60 | 6 | Low | Low | Delayed-enhance | Breathless | – | – | + | 0.79 |
| 3 | 60 | 24 | Normal | Low | Normal | None | – | + | + | 0.87 |
| 4 | 60 | 5 | Normal | Low | T2WI high | None | – | – | + | 0.80 |
| 5 | 60 | 36 | Normal | Normal | Delayed-enhance | Chest pain | – | + | + | 0.74 |
| 6 | 70 | 65 | Low | Low | Normal | Breathless | – | – | – | 0.43 |
| 7 | 60 | 5 | Low | Low | Normal | Breathless | – | – | + | 0.73 |
| 8 | 60 | 34 | Low | Low | Normal | Chest pain | – | – | + | 0.66 |

*Abbreviations:* LVEF = left ventricular ejection fraction; Gd-MRI = gadolinium-magnetic resonance imaging.

Five patients showed low $^{123}$I-BMIPP accumulation and four patients showed low $^{201}$TlCl accumulation in the base of the left ventricular myocardium corresponding to high FDG accumulation regions. In two patients (2 and 5) delayed contrast MRI showed delayed enhancement in parts of the regions with high FDG accumulation, and Patient 5 showed T2WI high signal without delayed enhancement. $^{123}$I-BMIPP SPECT was not performed in Patient 6.

dial and myocardial fibrosis (6). An autopsy study of patients irradiated with at least 35 Gy (mean dose of 56 Gy to the anterior heart surface) showed that 50% of the cases had myocardial fibrosis, 75% had fibrous thickening of the mural endocardium, and 90% had pericardial thickening (1). These studies indicate the possibility of radiation causing crucial damage to the heart.

We could demonstrate the time-course of irradiation on the myocardium on FDG-PET in Fig. 4. The patient had been treated with chemoradiotherapy for postoperative recurrent esophageal cancer and showed normal FDG uptake in the myocardium at one month after the completion of chemoradiotherapy. However, at five months after the completion of chemoradiotherapy, he showed high FDG uptake and low uptake of both $^{123}$I-BMIPP and $^{201}$TlCl in the basal myocardium, which was located inside the high-dose irradiated field. These findings suggest that abnormal FDG-PET findings in the heart might not be shown until several months after the completion of radiation therapy and indicate that increasing glucose metabolism might be a late adverse event caused by radiation.

Magnetic resonance imaging is thought to be able to reveal myocardial damage as delayed enhancement on Gd-DTPA-enhanced T1-weighted images. These findings suggest myocardial damage due to ischemia or other nonischemic cardiomyopathies but are not specific to disease. The finding of delayed enhancement is thought to be related to an increase in volume distribution of gadolinium secondary to interstitial space expansion, which occurs in a state of fibrous scarring or inflammation. Our MRI results showed delayed enhancement in portions of the high FDG uptake areas in only two patients. MRI findings are not thought to be sensitive and may reflect a later-phase condition of myocardial damage. It is possible that abnormalities cannot be detected by US until myocardial fibrosis further progresses.

Myocardial SPECT studies may demonstrate functional changes with higher sensitivity than MRI. In this study, six of the eight patients showed decreased perfusion and/or fatty acid metabolism in the basal myocardium. However, decreased uptake in the basal portion is often recognized as attenuation artifacts and is hardly able to be detected as abnormal findings on SPECT. On the other hand, FDG-PET can detect such changes as clear "hot spots." These findings are very helpful for visual detection of abnormalities. However, there were some cases in which the myocardium showed diffuse high FDG uptake, even under the condition of more than four hours of fasting. These findings often mimic abnormal focal high uptake in the heart. This might be one of the limitations of FDG-PET.

With the development of technology and accuracy of radiotherapy, prognosis of malignant tumors has improved. More attention must therefore be paid to long-term toxicities such as radiation-induced myocardial damage. We reported in 2000 that 15 of 238 patients with superficial esophageal cancer who had been irradiated died due to heart disease, and Ishikura *et al.* also reported in 2002 that four of 78 patients with esophageal cancer who had remained in complete response with chemoradiotherapy died as a result of heart disease (17, 18). More-

over, the rate of heart-related deaths in patients with breast cancer who underwent preventive radiotherapy after left breast-conserving surgery was reported to be higher than in patients who underwent preventive radiotherapy after right breast-conserving surgery (2). The increase in overall survival in some trials achieved by locoregional treatment of breast cancer appeared to be counterbalanced by an increase in late cardiac mortality (2–5). Radiation-induced myocardial damage may account for some proportion of cardiac events and become one of the prognostic factors for patients with esophageal cancer after chemoradiotherapy. Moreover, in the present study, three of the eight patients with high FDG uptake in the basal myocardium had no symptoms, suggesting that radiation-induced myocardial damage might progress slowly and hardly cause symptoms in the early stages. Thus, early detection of radiation-induced myocardial damage is thought to be important for the improvement of prognosis. Although there was no relationship between high FDG accumulation and dose-volume of the left ventricle in the present study, Gyenes et al. and Rutqvist et al. analyzed mortality from ischemic heart disease according to estimated heart dose-

volume and found that the cumulative mortality rate was significantly higher in patients in the high-dose–volume subgroup than in patients who received no radiotherapy (21, 22). Thus, radiation–oncologists may have to make efforts to reduce irradiated cardiac volume to minimize the risk of radiation-associated adverse events.

However, in this study, we could not determine the correlation between those findings on FDG-PET (including SUV) and pathology. In addition, we could not follow the changes of those findings on FDG-PET. Further studies are needed to clarify the relationship between FDG-PET findings and risk of myocardial damage.

## CONCLUSIONS

Focal increased FDG uptake in the basal myocardium is sometimes seen in patients with esophageal cancer after radiotherapy. This finding might indicate radiation-induced myocardial damage. Cardiac function and symptom of the patients with those focal increased FDG uptake should be followed to prevent cardiac impairment or death as a result of radiation therapy.

## REFERENCES

1. Brosius FC 3rd, Waller BF, Roberts WC. Radiation heart disease. Analysis of 16 young (aged 15 to 33 years) necropsy patients who received over 3,500 rads to the heart. Am J Med 1981;70:519–530.
2. Paszat LF, Mackillop WJ, Groome PA, et al. Mortality from myocardial infarction following postlumpectomy radiotherapy for breast cancer: A population-based study in Ontario, Canada. Int J Radiat Oncol Biol Phys 1999;43:755–762.
3. Early Breast Cancer Trialists' Collaborative Group. Favourable and unfavourable effects on long-term survival of radiotherapy for early breast cancer: An overview of the randomised trials. Lancet 2000;355:1757–1770.
4. Cuzick J, Stewart H, Rutqvist L, et al. Cause-specific mortality in long-term survivors of breast cancer who participated in trials of radiotherapy. J Clin Oncol 1994;12:447–453.
5. Kuske RR. Adjuvant chest wall and nodal irradiation: Maximize cure, minimize late cardiac toxicity. J Clin Oncol 1998; 16:2579–2582.
6. Lauk S, Kiszel Z, Buschmann J, et al. Radiation-induced heart disease in rats. Int J Radiat Oncol Biol Phys 1985;11:801–808.
7. Maunoury C, Pierga JY, Valette H, et al. Myocardial perfusion damage after mediastinal irradiation for Hodgkin's disease: A thallium-201 single photon emission tomography study. Eur J Nucl Med 1992;19:871–873.
8. Hardenbergh PH, Munley MT, Bentel GC, et al. Cardiac perfusion changes in patients treated for breast cancer with radiation therapy and Doxorubicin: Preliminary results. Int J Radiat Oncol Biol Phys 2001;49:1023–1028.
9. Gyenes G, Fornander T, Carlens P, et al. Detection of radiation-induced myocardial damage by technetium-99m sestamibi scintigraphy. Eur J Nucl Med 1997;24:286–292.
10. Fuller SA, Haybittle JL, Smith RE, et al. Cardiac doses in postoperative irradiation. Radiother Oncol 1992;25:19–24.
11. Gyenes G, Fornander T, Carlens P, et al. Morbidity of ischemic heart disease in early breast cancer 15–20 years after adjuvant radiotherapy. Int J Radiat Oncol Biol Phys 1994;28: 1235–1241.
12. Baum M. The Skinner lecture: A cost-benefit analysis postoperative radiotherapy in the treatment of early breast cancer. Clin Oncol 1991;3:223–229.
13. Cuzick J, Stewart H, Rutqvist L, et al. Cause-specific mortality in long-term survivors of breast cancer who participated in trials of radiotherapy. J Clin Oncol 1994;12:447–453.
14. Gustavsson A, Eskilsson J, Landberg T, et al. Late cardiac effects after mantle radiotherapy in patients with Hodgkin's disease. Annals of Oncology 1990;1:355–366.
15. Glanzmann C, Kaufmann P, Jenni R, et al. Cardiac risk after mediastinal irradiation for Hodgkin's disease. Radiother Oncol 1998;46:51–62.
16. Boivin JF, Hutchison GB, Lubin JH, et al. Coronary artery disease mortality in patients treated for Hodgkin's disease. Cancer 1992;69:1241–1247.
17. Yamada S, Nemoto K, Takai Y, et al. Proposal for standard radiotherapy methods for superficial esophageal cancer. A multicenter retrospective evaluation. J JASTRO 2000;12:169–176.
18. Ishikura S, Nihei K, Ohtsu A, et al. Long-term toxicity after definitive chemoradiotherapy for squamous cell carcinoma of the thoracic esophagus. J Clin Oncol 2003;21:2697–2702.
19. Mukherjee S, Aston D, Minett M, et al. The significance of cardiac doses received during chemoradiation of oesophageal and gastro-oesophageal junctional cancers. Clin Oncol 2003; 15:115–120.
20. Keiichi J, Kenji N, Tomohiro K, et al. A case of high FDG-uptake into the myocardium after radiotherapy for esophageal cancer. Nippon Igaku Hoshasen Gakkai Zasshi 2005;65:266–269.
21. Rutqvist LE, Lax I, Fornander T, et al. Cardiovascular mortality in a randomized trial of adjuvant radiation therapy versus surgery alone in primary breast cancer. Int J Radiat Oncol Biol Phys 1992;22:887–896.
22. Gyenes G, Rutqvist LE, Liedberg A, et al. Long-term cardiac morbidity and mortality in a randomized trial of pre- and postoperative radiation therapy versus surgery alone in primary breast cancer. Radiother Oncol 1998;48:185–190.

# Investigations of different kilovoltage x-ray energy for three-dimensional converging stereotactic radiotherapy system: Monte Carlo simulations with CT data

Hossain M. Deloar[a)]
*Department of Radiology, Keio University, Tokyo, Japan and CREST, Japan Science and Technology Agency, Tokyo, Japan*

Etsuo Kunieda[b)] and Takatsugu Kawase
*Department of Radiology, Keio University, Tokyo, Japan*

Takanori Tsunoo
*Department of Radiology, Keio University, Tokyo, Japan and CREST, Japan Science and Technology Agency, Tokyo, Japan*

Hidetoshi Saitoh
*Department of Radiological Sciences, Tokyo Metropolitan University of Health Sciences, Tokyo, Japan*

Masahiro Ozaki
*CT Systems Division, Toshiba Medical Systems Corporation, Tokyo, Japan*

Kimiaki Saito
*Center for Promotion of Computational Science and Engineering, Japan Atomic Energy Agency, Ibaraki, Japan*

Shunji Takagi and Osamu Sato
*Safety Engineering and Technology Department, Mitsubishi Research Institute, Tokyo, Japan*

Tatsuya Fujisaki
*Department of Radiological Sciences, Ibaraki Prefectural University of Health Sciences, Ibaraki, Japan*

Atsushi Myojoyama
*Department of Radiological Sciences, Tokyo Metropolitan University of Health Sciences, Tokyo, Japan*

Graham Sorell
*Department of Medical Physics and Bioengineering, Christchurch Hospital, Christchurch, New Zealand*

We are investigating three-dimensional converging stereotactic radiotherapy (3DCSRT) with suitable medium-energy x rays as treatment for small lung tumors with better dose homogeneity at the target. A computed tomography (CT) system dedicated for non-coplanar converging radiotherapy was simulated with BEAMnrc (EGS4) Monte-Carlo code for x-ray energy of 147.5, 200, 300, and 500 kilovoltage (kVp). The system was validated by comparing calculated and measured percentage of depth dose in a water phantom for the energy of 120 and 147.5 kVp. A thorax phantom and CT data from lung tumors ($<20$ cm$^3$) were used to compare dose homogeneities of kVp energies with MV energies of 4, 6, and 10 MV. Three non-coplanar arcs ($0°$ and $\pm 25°$) around the center of the target were employed. The Monte Carlo dose data format was converted to the XiO RTP format to compare dose homogeneity, differential, and integral dose volume histograms of kVp and MV energies. In terms of dose homogeneity and DVHs, dose distributions at the target of all kVp energies with the thorax phantom were better than MV energies, with mean dose absorption at the ribs (human data) of 100%, 85%, 50%, 30% for 147.5, 200, 300, and 500 kVp, respectively. Considering dose distributions and reduction of the enhanced dose absorption at the ribs, a minimum of 500 kVp is suitable for the lung kVp 3DCSRT system. © *2006 American Association of Physicists in Medicine.* [DOI: 10.1118/1.2361080]

## I. INTRODUCTION

Stereotactic radiotherapy (SRT) and stereotactic radiosurgery often utilize multiple non-coplanar oblique beams to avoid critical structures and maximize target coverage. Accuracy of therapeutic effectiveness in stereotactic radiotherapy (SRT) depends on stereotactic localization techniques with fractionated radiation delivery to tumors.[1-8] With SRT treatment of small lung tumors, a common method of beam collimation is to use a circular collimator that can be rigidly attached to the linear accelerator head (linac).[9] The ability to deliver a homogeneous dose distribution within the tumor is complicated by differences in density between tumor tissue and surrounding lung tissue because of the effect of increased electron range and reduced photon attenuation.[10]

To treat deep-seated tumors, photons of higher energy are often preferred. For lung tumors, as photon energy increases,

**Target**
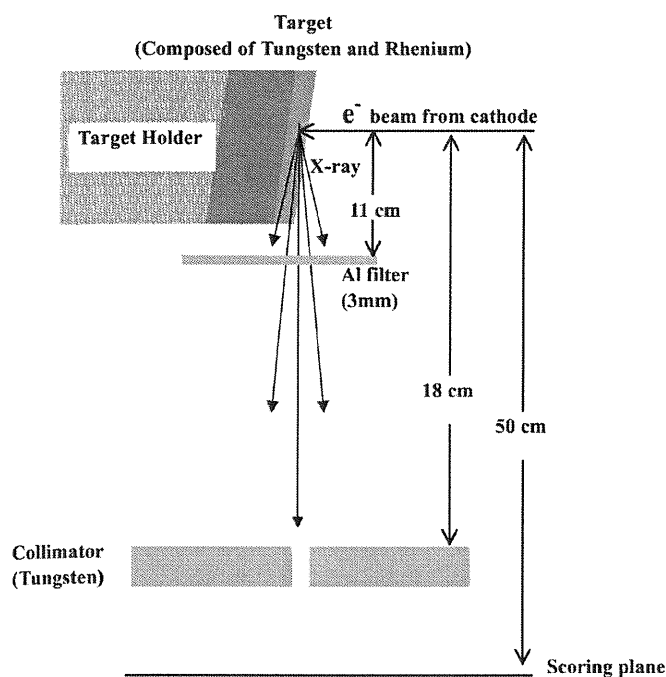**(Composed of Tungsten and Rhenium)**



FIG. 1. Geometry of the x-ray tube in CT simulated with Monte Carlo technique. Target was a mixture of tungsten and rhenium, with copper used as the target holder. Collimator material was tungsten. Thickness of Al filter was 3 mm, and various x-ray energies were sampled at the scoring plane (phase-space file). The collimator was opened for the 2 cm × 2 cm beam size at 50 cm source-surface distance (SSD).

distributions of lateral scatter electrons are increased in normal lung due to low tissue densities (0.1–0.3 g/cm$^3$) and the lateral scatter of electrons out of the beam path, which can also lead to loss of field flatness and increased penumbra width.[11–15] In Monte Carlo (MC) simulations for stereotactic irradiation using a variety of photon energies, it has been shown that with increasing x-ray energy, dispersion of absorbed dose in small lung tumors (2 cm $\phi$) increases. In contrast the dose uniformity within the tumor increases as x-ray energy decreases.[16]

With an x-ray energy of 140 kilovoltage peak (kVp), a conventional computed tomography (CT) scanner has been used as a therapy machine by adding a collimator to produce rectangular or square radiation fields.[17] Such a machine has been used as arc therapy to treat brain tumors in animals[18] and humans[19] with infusion of x-ray contrast materials to enhance radiation dose.

We are investigating the possible use of a three-dimensional converging stereotactic radiotherapy (3DCSRT) system to treat small lung tumors with kilovoltage x-ray energy by modifying the necessary hardware of a conventional CT system. Usually kilovoltage x-ray energy incident from a single direction has higher absorption near the body surface; however, using a technique converging non-coplanar multiple arcs can produce a much higher dose to a deep-seated target than to the body surface. Usual CT systems use an energy range of 100–150 kVp. One problem in treating lung tumors with low-energy kilovoltage x rays is high dose absorption at the ribs due to high sensitivity for bone. Although

contrast material can enhance the dose at a brain target and thereby minimizing the relative effect on bone,[19] an ideal contrast material for lung has not yet become available. Therefore, the only way to avoid dose absorption at the ribs is to increase the x-ray energy of the system.

In our previous study,[20] we modeled a conventional CT system for various energy spectra of 100–500 kVp with Monte Carlo technique. Dosimetry of a 3DCSRT system with converging non-coplanar multiple arcs are yet to be investigated. In this study, we investigated the dosimetry properties of our 3DCSRT system with Monte Carlo simulation[21] for x-ray energy of 147.5, 200, 300, and 500 kVp in a thorax phantom and human lung in terms of dose distribution and dose volume histogram (DVH) on a dedicated radiation treatment planning (RTP) system. Those results are compared with linear energy accelerator (linac) energy of 4, 6, and 10 MV. This study will help us to determine the necessary changes to CT hardware (e.g., the x-ray tube) to achieve suitable energy for our 3DCSRT system. In reality, current commercial CT scanners do not have the capability to make a noncoplanar arc and CT scanner design needs to be modified to allow limited table-top rotation along the isocenter to satisfy the beam configuration we used for our simulation.

## II. MATERIALS AND METHODS

### A. X-ray tube simulation

The BEAMnrc Monte Carlo user code was developed to simulate photon and electron beams produced by linear accelerators used in radiotherapy[21] and recent versions of the code (BEAMnrcMP) can also accurately model low-energy photons. The geometry of various components of the accelerator is modeled by a series of independent component modules. In our previous study,[20] we modeled the x-ray tube of a CT system (Toshiba Aquilion TSX-101A, Japan) for various energies (100, 120, 147.5, 200, 300, 400, and 500 kVp) with the component module XTUBE currently available within the BEAMnrc system. Information of particles transports phenomena in simulations was stored in the phase space file (scoring plan) below the collimator. The simulated geometry of this system is shown in Fig. 1. The target in the x-ray tube was composed of tungsten and rhenium. To make a narrow beam, a tungsten collimator was designed to open in such a way that it gave a 2 cm × 2 cm or 3 cm × 3 cm beam at a 50 cm source-to-surface distance (SSD). Source-to-collimator distance was 18 cm, and an Al filter of 3 mm thickness was used. The global electron and photon cutoff energies used in the simulation were 0.05 and 0.001 MeV, respectively, and 300 × 10$^6$ electron events were used in all cases. The uncertainty in the fluence distributions was around 2% in the penumbra region, and less than 0.5% inside the field. All Monte Carlo calculations in this study were performed using a cluster unit of 12 PC.